Advanced Composite Materials
Publication details, including instructions for authors and subscription information:
http://www.tandfonline.com/loi/tacm20

Experimental and Numerical Simulation Studies of Low-Velocity Impact Responses on Sandwich Panels for a BIMODAL Tram

Jae-Youl Lee [a] , Kwang-Bok Shin [b] & Jong-Cheol Jeong [c]

[a] Graduate School of Mechanical Engineering, HANBAT National University, San 16-1, Dukmyung-Dong, Yuseong-Gu, Daejon 305-719, Korea

[b] Division of Mechanical Engineering, HANBAT National University, San 16-1, Dukmyung-Dong, Yuseong-Gu, Daejon 305-719, Korea;, Email: shin955@hanbat.ac.kr

[c] Transit Division, HanKuk Fiber Glass Co., Ltd., 181-1, Yonji-Ri, Bubuk-Myun, Milyang-Shi, Kyungnam 627-850, Korea

Version of record first published: 02 Apr 2012.

VSP

Advanced Composite Materials 18 (2009) 1–20

ADVANCED COMPOSITE MATERIALS
www.brill.nl/acm

Experimental and Numerical Simulation Studies of Low-Velocity Impact Responses on Sandwich Panels for a BIMODAL Tram

Jae-Youl Lee [a], **Kwang-Bok Shin** [b,*] **and Jong-Cheol Jeong** [c]

[a] Graduate School of Mechanical Engineering, HANBAT National University, San 16-1, Dukmyung-Dong, Yuseong-Gu, Daejon 305-719, Korea
[b] Division of Mechanical Engineering, HANBAT National University, San 16-1, Dukmyung-Dong, Yuseong-Gu, Daejon 305-719, Korea
[c] Transit Division, HanKuk Fiber Glass Co., Ltd., 181-1, Yonji-Ri, Bubuk-Myun, Milyang-Shi, Kyungnam 627-850, Korea

Received 26 October 2007; accepted 14 January 2008

Abstract

This paper describes the results of experiments and numerical simulation studies on the impact and indentation damage created by low-velocity impact subjected onto honeycomb sandwich panels for application to the BIMODAL tram. The test panels were subjected to low-velocity impact loading using an instrumented testing machine at six energy levels. Contact force histories as a function of time were evaluated and compared. The extent of the damage and depth of the permanent indentation was measured quantitatively using a 3-dimensional scanner. An explicit finite element analysis based on LS-DYNA3D was focused on the introduction of a material damage model and numerical simulation of low-velocity impact responses on honeycomb sandwich panels. Extensive material testing was conducted to determine the input parameters for the metallic and composite face-sheet materials and the effective equivalent damage model for the orthotropic honeycomb core material. Good agreement was obtained between numerical and experimental results; in particular, the numerical simulation was able to predict impact damage area and the depth of indentation of honeycomb sandwich composite panels created by the impact loading.

Keywords

BIMODAL tram, effective damage model, explicit finite element analysis, honeycomb sandwich composite, low-velocity impact

* To whom correspondence should be addressed. E-mail: shin955@hanbat.ac.kr
Edited by the KSCM
Translated paper originally published in the *Journal of the Korean Society for Composite Materials*

 DOI:10.1163/156855108X385311

1. Introduction

Ground transportation vehicles should be designed to be of sufficient strength, to have the lowest possible vehicle resistance, to be made of lightweight construction and to lay the specified load gauge or roadway. Lightweight design and a significant reduction of the production costs are the driving factors for the introduction of new material systems in ground transportation applications. Therefore, the use of composites in ground transportation vehicles has increased quite substantially in recent years as designers have come to appreciate the benefits afforded by such systems [1]. In particular, the use of sandwich composite structures in Korea has been proposed and recommended in ground transportation applications such as the tilting train, and low-floor bus and tram vehicles because lighter vehicles would increase energy efficiency and yield capacity increase by providing increased payload [2, 3].

Until recently, several countries have been developing advanced thermoplastic composite materials and manufacturing technologies to reduce the weight of tram vehicles. The design, analysis, process modeling, manufacturing concepts and prototypes that provide form-fit function and performance validation have now all been demonstrated for the car-body component of a tram vehicle [4].

The BIMODAL tram project offers an environmentally friendly alternative to conventional transport, and is being developed with options for zero emission drive systems, wire guided steering, and electric and hydrogen fuel cell powered options. In particular, the BIMODAL tram is a development project subjected to weight limit regulation by Government. The BIMODAL tram has the advantage of faster boarding and alighting for the majority of passengers including the elderly and disabled, as well as elimination of the wheelchair lift due to low-floor when compared to conventional transports. Also, the BIMODAL tram can travel autonomously on roadways like buses or along dedicated alignments and through pedestrian areas using concealed wire guidance.

The BIMODAL tram will be developed using sandwich composite panels with high stiffness-to-weight and strength-to-weight ratios and low manufacturing investment cost to reduce the weight of the vehicle. The sandwich constructions are considering as the best material systems to meet the weight requirements. However, sandwich panels are known to be susceptible to impact damage by foreign objects that are expected during the life of the structure. Impact induced damage can cause drastic decrease in the strength of the structure. Impact may come from a variety of causes. Typically, low-velocity impact may result from tool drops, hail and debris thrown up from runways.

Schubel *et al.* [5] studied experimentally the low-velocity impact behavior of simply supported sandwich panels consisting of woven carbon/epoxy face-sheets and a PVC foam core. Results have been compared with those of an equivalent static loading and showed that low-velocity impact was generally quasi-static in nature except for localized damage. Anderson and Madenci [6] conducted low-velocity impact tests to characterize the type and extent of the damage observed in a variety of sandwich configurations with graphite/epoxy face-sheets and foam or

honeycomb cores. They found that correlation of the residual indentation and cross-sectional views of the impacted specimens provided a criterion for the extent of the damage. Horrigan *et al*. [7] conducted experimental and theoretical investigations on low-velocity impact response of a Nomex honeycomb sandwich structure with glass fiber-reinforced epoxy resins. They showed that a soft, compliant projectile results in shallow crushing of the core whereas hard bodies create deeper damage that conforms to the shape of the projectile. Meo *et al.* [8], Hoo and Park [9] and Davies *et al.* [10] carried out experimental and analytical investigations on low-velocity impact response of composite sandwich structures. They showed that several common failure modes have been identified, including core indentation/cracking, face-sheet buckling, delamination within the face-sheet, and debonding between the face-sheet and core.

Although much research already exists on the study of low-velocity impact of sandwich panels, new configurations are continually being developed and need to be characterized because predictions of the effects of low-velocity impact damage are difficult and are still relatively immature [11].

The objectives of this study are to understand the impact-damage mechanism, the load distribution in the composite and metallic face-sheet of the sandwich panel, and to determine the failure mechanisms and to construct an effective damage model of a honeycomb sandwich panel. Experimental data were generated using an instrumented test machine to create the impact damage. A 3-dimensional scanner was utilized to measure quantitatively the impacted damage size and depth of the permanent indentation created by low-velocity impacts. The numerical study consisted of finite element analyses of the low-velocity impact of a honeycomb sandwich panel using LS-DYNA3D. Experimental results with respect to dent depth and damage area created by impact loading were compared with finite element analysis results.

2. Material Systems for BIMODAL Tram

The BIMODAL tram will be developed using a hybrid design concept combined with honeycomb sandwich and laminated composite structures as shown in Fig. 1. The sandwich constructions are being considered for application to primary structures such as body-shell, roof and floor, while laminated composites are being applied only for the components of relatively high curvatures and complex geometry which are more troublesome to be manufactured using the sandwich panels.

The sandwich panels are classified into two groups according to the part of application in the BIMODAL tram. One group is the sandwich panels for application to body-shell structures that would be composed of the woven glass fabric/epoxy laminate face-sheet and aluminum honeycomb core. The second group is the sandwich panels for application to floor structures that would be made of the aluminum 5052 face-sheet and aluminum honeycomb core. Table 1 summarizes the types of sandwich panels that would be applied to body-shell and floor structures in BIMODAL tram.

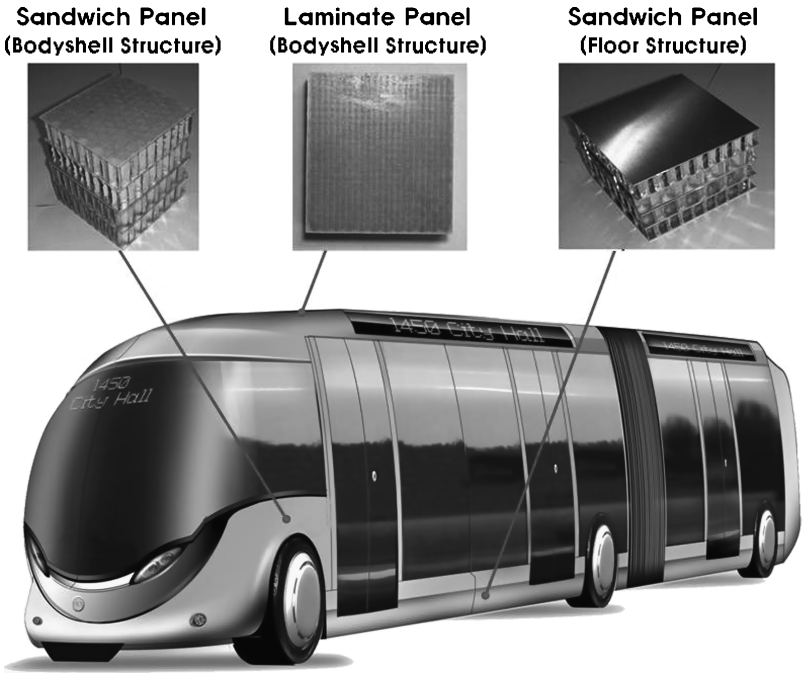

Figure 1. Design concept of BIMODAL tram vehicle.

Table 1.
The types of sandwich panels considered in design stage

Applied part	Name	Face-sheet material	Core material	Thickness (mm), $t_1/t_c/t_2$
Body-shell	GE/AH	**G**lass fabric/**E**poxy (WR580/NF4000)	**A**luminum 5052 **H**oneycomb (3/8″–5052-0.0025″)	3.0/25.4/1.5
Floor	AL/AH	**AL**uminum 5052	**A**luminum 5052 **H**oneycomb (3/8″–5052–0.0025″)	1.2/16.0/1.2

* t_1 — outer face-sheet, t_2 — inner face-sheet, t_c —core.

For sandwich panels used in body-shell structures, the outer face-sheet has a thickness that is twice the thickness of the inner face-sheet to achieve the additional cost and weight savings. The face-sheets of sandwich panel for application to body-shell structures are laminates made of the woven glass fabric/epoxy prepreg. This glass fabric was five-hardness satin weaves with the same tow count in the warp and fill direction. The woven glass fabric/epoxy laminate have the dimensions of sandwich with face-sheets of unequal thickness. The face-sheets of sandwich panels for application to the floor structures are a metal material made of aluminum 5052 and have the same thickness for outer and inner face-sheets. The core used in body-shell sandwich panels is an aluminum honeycomb of 25.4 mm thickness, while an

aluminum honeycomb of 16.0 mm thickness is chosen as the core materials of floor sandwich panels.

3. Experimental and Numerical Simulation Procedures

3.1. Low-Velocity Impact Test

All sandwich panels were fabricated by bonding the face-sheets to the core material with Bondex® 606 adhesive film, a high temperature curing epoxy resin. The face-sheets and core were bonded together and cured in autoclave according to curing cycle in Fig. 2. The curing cycle consisted of a 2.5°C/min ramp to 80°C and 1.5°C/min ramp to 127°C, where the sandwich panel was cured under vacuum for 6 h. Once the curing process of sandwich panels was complete, 100 × 100 mm test specimens were cut and prepared to test.

Impact tests were performed using the instrumented impact testing system, Dynatup model 8250, which consists of a drop tower equipped with an impactor and a variable cross-head weight arrangement, a high speed data acquisition system, and a load transducer mounted in the impactor as shown in Fig. 3. The impactor end had an instrumented hemispherical tip of diameter 15.86 mm and the impactor weight was kept constant at 1.95 kg for all tests. The sandwich panels were subjected to impact with increasing drop heights. The panel was a circular air cylinder in clamped condition during the low-velocity impact event. After initial contact, pneumatic rebound brakes prevent repeated impacts. After the completion of the impact tests, the barely visible impact damage size and depth of the permanent indentation was measured precisely using a 3-D scanner. The panels of size 100 × 100 mm were tested at impact energy range of 1.3–6.0 J, which represents the range that a typ-

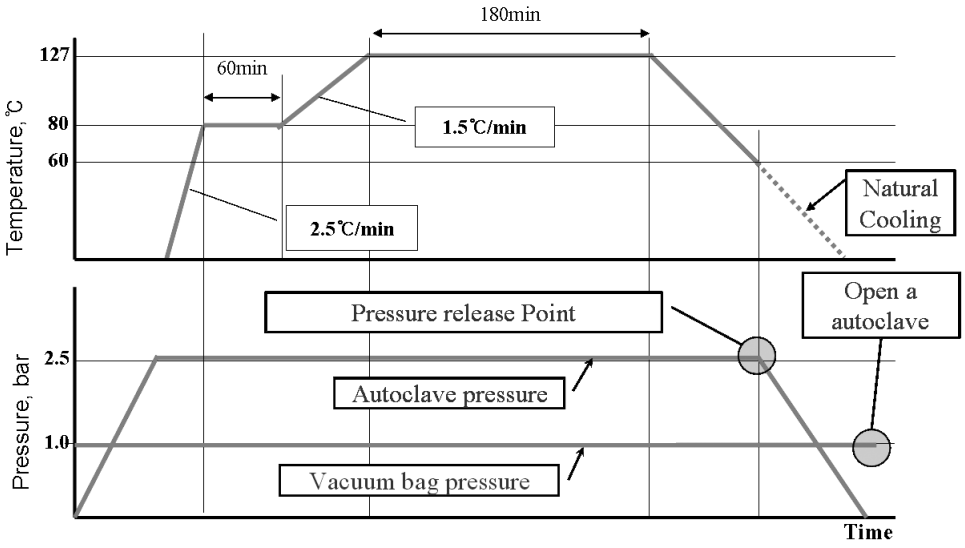

Figure 2. Autoclave curing cycle.

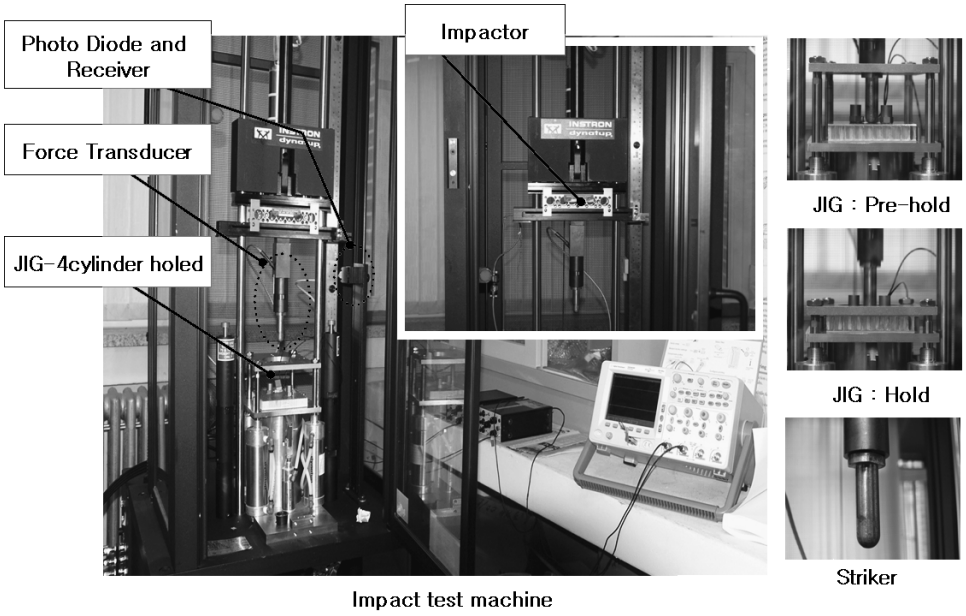

Figure 3. Impact test machine.

Table 2.
The impact energies of body-shell and floor sandwich panels

	GE/AH (Body-shell sandwich panel)	AL/AH (Floor sandwich panel)
Impact energy (J)	1.31	1.57
	3.17	3.04
	4.13	4.49
	6.00	5.93

ical tram transit experiences under low-velocity impact. The sandwich specimens for application to the body-shell and floor structure were tested under low-velocity impact conditions in Table 2. The small differences of impact energy applied to the body-shell and floor sandwich specimens in Table 2 are due to the different thickness and test conditions between sandwich specimens of the two groups, although the drop height is equal.

3.2. Numerical Simulation

3.2.1. Effective Damage Model

During impact of a projectile on a sandwich panel, the target experiences localized deformation in the vicinity of the point of impact as well as overall structural deformation. The localized deformation in a sandwich panel could be estimated from a large-scale numerical analysis of the dynamic contact problem and by introducing

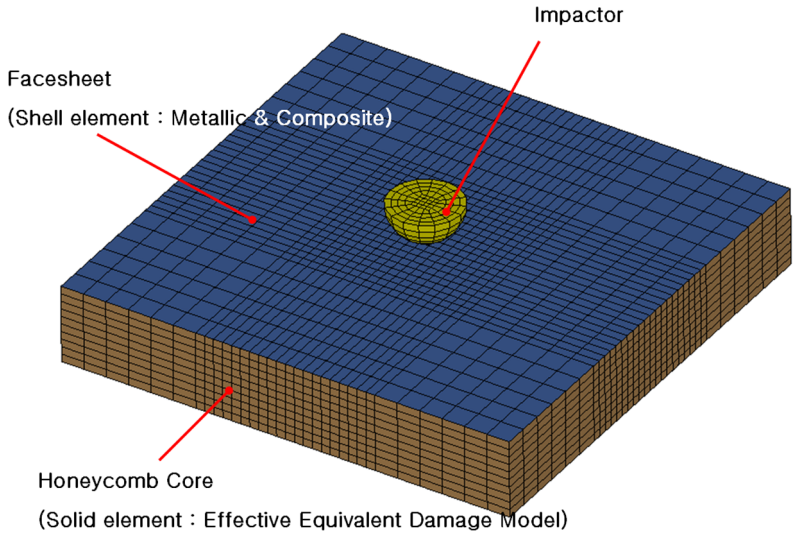

Figure 4. The finite element model of the honeycomb sandwich panels. This figure is published in color on http://www.ingentaconnect.com/content/vsp/acm

a contact law that accounts for the effect of inelastic deformation and damage induced in the impact zone. In this study, the damage area in the sandwich panel after impact loading was analyzed using the explicit finite element code LS-DYNA3D. The finite element model of the undamaged panel is shown in Fig. 4.

The sandwich panel was modeled as a combination of solid and shell elements. A four-node Belytschko–Tsai shell element was used for modeling the composite and metallic face-sheet while eight node solid elements were employed to model the effective equivalent honeycomb core. The adhesive film layers were not considered in the finite element model because the adhesive film was too thin to be modeled using a solid element and it was bonded strongly at each of the interfaces. Different approaches for modeling of the honeycomb core with the configuration of the hexagonal cell by the finite element method do exist, which differ in modeling time, computational cost and accuracy of the results and their adoption depends on the specific model size and loading case. A detailed representation of the hexagonal cells with shell elements can predict the cell wall deformation for impact simulations reasonably well, but is unsuitable for large scale models due to the computational cost [12, 13].

3.2.2. Loading and Contact Conditions

Load was applied to the model by specifying an initial velocity of the impactor. The impacting speed was obtained by measurement with a photodiode. The support boundary conditions were specified between support jig and face-sheet. A rigid material model was assumed for the impactor.

A surface contact algorithm is used to simulate contact between the impacting body and the top face-sheet. The modeling of the contact-impact problem is gov-

erned by the fact that the impacting body and the target must not penetrate each other. This condition was achieved by using the symmetric penalty method, and a symmetric surface-to-surface contact algorithm was assumed. The major difficulty in solving the contact problem is the assignment of the value of the normal penalty stiffness which affects the accuracy and stability of the solution. The penalty algorithm has the main drawback that an increase of the penalty stiffness reduces the stable time increment, since the penalty springs increase the overall stiffness acting on the interface nodes [14]. In order to find a reasonable value of the penalty stiffness factor in contact surfaces, several runs were conducted. The right value of penalty stiffness factor was 0.2 for this study.

3.2.3. Material Model of Aluminum 5052 Face-Sheet

The LS-DYNA3D material model #24 (*MAT_PIECEWISE_LINEAR_PLASTICTIY) was used for the aluminum 5052 face-sheet material of shell element. These materials are defined in stress–strain curve obtained by tensile test, the properties of which are presented in Table 3.

3.2.4. Material Model of Aluminum Honeycomb Core

For reasons of simplification, the cellular honeycomb core structure was treated as a homogeneous material using its effective orthotropic material properties. The honeycomb material directions are defined as the x-direction (ribbon direction), y-direction (direction perpendicular to the ribbon) and z-direction (thickness direction) as shown in Fig. 5.

The LS-DYNA3D material model #126 (*MAT_MODIFIED_HONEYCOMB) was used for the honeycomb core material of the solid element. In this orthotropic

Table 3.
Material properties of aluminum 5052

Density (kg/m^3)	Elastic modulus (GPa)	Poisson's ratio	Yield stress (MPa)	Tangent modulus (GPa)
2,750	70.0	0.33	193.0	49.0

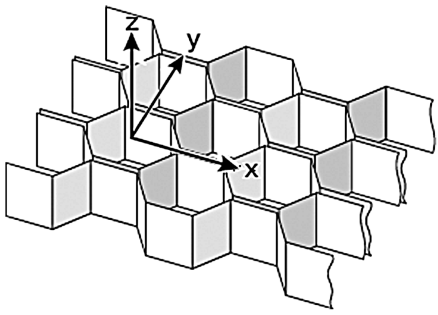

Figure 5. Honeycomb material directions.

material model, nonlinear elastoplastic constitutive behavior based on the experimentally determined stress–strain curve can be defined for the z-direction as shown in Fig. 6. The z-direction compressive stress–strain curve for honeycomb cores can be divided into three distinct regions: (1) at low strains a linearly elastic region, (2) a region corresponding to progressive crushing at nearly constant stress level and (3) a region of rapidly increasing stresses with further deformation due to the fact that the cell walls are forced into contact with each other. The effective orthotropic material properties of honeycomb core are shown in Table 4.

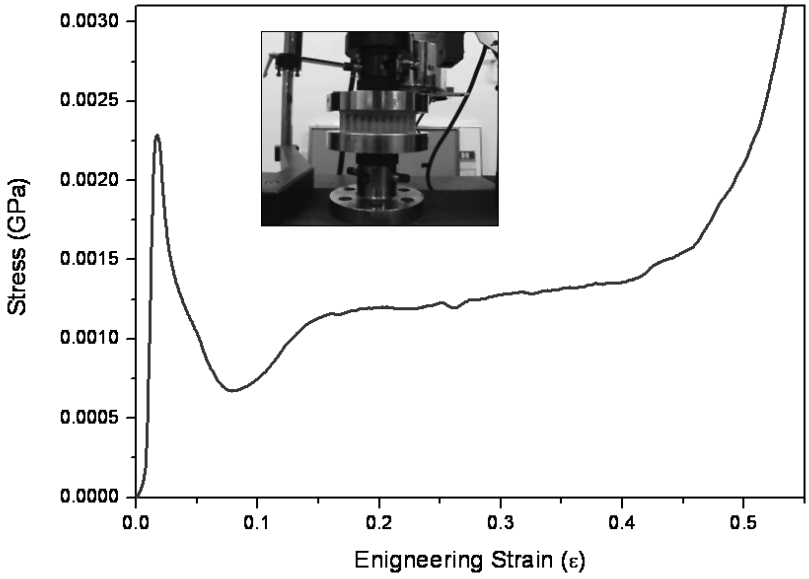

Figure 6. The stress–strain curve for aluminum honeycomb core (z-direction).

Table 4.
The effective orthotropic material properties of aluminum honeycomb core

Properties	Value
Density (kg/m^3)	59.26
Young's modulus for honeycomb material (GPa)	70
Poisson's ratio for honeycomb material	0.33
Elastic modulus, E_x (GPa)	0.33×10^{-3}
Elastic modulus, E_y (GPa)	0.33×10^{-3}
Elastic modulus, E_z (GPa)	1.37
Shear modulus, G_{xy} (GPa)	0.18×10^{-1}
Shear modulus, G_{yz} (GPa)	0.18
Shear modulus, G_{xz} (GPa)	0.18

3.2.5. Material Model of WR580/NF4000 Composite Laminate Face-Sheet

The damage to a composite laminate due to transverse impact loading generally involves several modes, such as matrix tensile cracking, matrix compressive and shear failure fiber matrix debonding, fiber breakage (tensile or compressive), delamination, etc. Among these damage modes, delamination is the most important mode for fiber-reinforced composites. Therefore, the glass/epoxy WR580/NF4000 composite laminate should be modeled as an orthotropic material with damage occurring by matrix cracking, compressive failure and fiber breakage.

The LS-DYNA3D material model #54 (*MAT_ENHANCED_COMPOSITE_DAMAGE) was used for the WR580/NF4000 glass fabric/epoxy face-sheet of the shell element. These constitutive models are based on the theory of continuum damage mechanics. It is assumed that the deformation of the materials introduces micro-cracks and cavities, which reduce the material stiffness. This is expressed through internal damage parameters which describe the evolution of the damage state under loading and hence the stiffness degradation [15].

The basis of the model is the modification made by Matzenmiller *et al.* [16] to the well-known Chang and Chang composite damage model [17]. The Chang and Chang failure criterion was utilized by the model to predict matrix cracking, compressive failure and fiber breakage of the laminate. The modified Chang and Chang failure criteria are shown in Table 5.

The sandwich face-sheets studied in this investigation are woven fabric laminates made of glass fiber-reinforced epoxy resin with a cure ply thickness of 3.0 mm for outer skin and 1.5 mm for inner skin. Tensile testing (ASTM D3039) and compression testing (ASTM D3410) in fill and warp direction as well as the determination of the shear properties (ASTM D5379) were performed to obtain elastic modulus, shear modulus, tensile and compressive strength in warp and fill direction, shear strength and Poisson's ratio. The WR580/NF4000 glass fabric/epoxy laminate material properties are shown in Table 6.

3.3. Experimental and Numerical Results

Contact force histories as a function of time for the body-shell sandwich specimens are presented in Fig. 7a. As observed in this figure, the peak contact force and contact time rise with impact energies for all specimens. The repeated rises and falls of the contact force histories reveal that failures occur successively in face-sheet and core materials during impact event. The load–time response up to the first peak load indicates an elastic response up to that point. Once the load reaches the first peak value, there is a sudden drop in the load, which indicates the notice of damage response in sandwich panels. The first load drop is due to the first type of failure such as delamination or fiber breakage in outer face-sheet made of composite laminate. The second and third peaks are due to the loading of the core and bottom face-sheet. The second and third load drops are due to the crushing of the core.

Contact force histories as a function of time for the floor sandwich specimens are shown in Fig. 7b. The peak contact force and contact time rise with impact energies,

Table 5.
The modified Chang–Chang failure criterion in LS-DYNA3D

Mode	Following conditions	
Fiber breakage	• *Tensile*, $\sigma_x > 0$	• *Compressive*, $\sigma_x < 0$
	$e_{\mathrm{ft}}^2 = \left(\frac{\sigma_x}{X_\mathrm{t}}\right)^2 + \left(\frac{\tau_{xy}}{S}\right) - 1,$	$e_{\mathrm{fc}}^2 = \left(\frac{\sigma_x}{X_\mathrm{c}}\right)^2 - 1,$
	where, $e_{\mathrm{ft}}^2 \geqslant 0$: failed and $e_{\mathrm{ft}}^2 \leqslant 0$: elastic	where, $e_{\mathrm{fc}}^2 \geqslant 0$: failed and $e_{\mathrm{fc}}^2 \leqslant 0$: elastic
Matrix cracking	• *Tensile*, $\sigma_x > 0$	• *Compressive*, $\sigma_x < 0$
	$e_{\mathrm{mt}}^2 = \left(\frac{\sigma_y}{Y_\mathrm{t}}\right)^2 + \left(\frac{\tau_{xy}}{S}\right) - 1,$	$e_{\mathrm{mc}}^2 = \left(\frac{\sigma_y}{2S_\mathrm{c}}\right)^2 + \left[\left(\frac{Y_\mathrm{c}}{2S_\mathrm{c}}\right)^2 - 1\right]\frac{\sigma_y}{Y_\mathrm{c}} + \left(\frac{\tau_{xy}}{S}\right)^2 - 1,$
	where, $e_{\mathrm{mt}}^2 \geqslant 0$: failed and $e_{\mathrm{mt}}^2 \leqslant 0$: elastic	where, $e_{\mathrm{mc}}^2 \geqslant 0$: failed and $e_{\mathrm{mc}}^2 \leqslant 0$: elastic
Fiber and matrix shearing	• *Tensile and compressive*	
	$e_{\mathrm{md}}^2 = \left(\frac{\sigma_y^2}{Y_\mathrm{c}Y_\mathrm{t}}\right)^2 + \left(\frac{\tau_{xy}}{S}\right)^2 + \frac{(Y_\mathrm{c} - Y_\mathrm{t})}{Y_\mathrm{c}Y_\mathrm{t}}\sigma_y - 1,$	
	where, $e_{\mathrm{md}}^2 \geqslant 0$: failed and $e_{\mathrm{md}}^2 \leqslant 0$: elastic	

σ_x, σ_y, τ_{xy} — stress of principal material direction; X_t, Y_t — tensile strength of fiber and matrix direction; Y_c, Y_c — compressive strength of fiber and matrix direction; S — in-plane shear strength; e — failure index; ft — fiber tensile; fc — fiber compressive; mt — matrix tensile; mc — matrix compressive; md — shearing mode of fiber and matrix.

Table 6.
Material properties of WR580/NF4000 glass fabric/epoxy laminate

Properties	Value
Density (kg/m^3)	1,830.00
Young's modulus — fill direction (GPa)	21.81
Young's modulus — warp direction (GPa)	18.71
Poisson's ratio between fill and warp direction	0.14
Shear modulus, G_{xy} (GPa)	4.53
Shear modulus, G_{yz} (GPa)	1.40
Shear modulus, G_{xz} (GPa)	1.40
Compressive strength — fill direction (MPa)	419.10
Compressive strength — warp direction (MPa)	439.12
Tensile strength — fill direction (MPa)	415.01
Tensile strength — warp direction (MPa)	421.95
Shear strength (MPa)	114.57

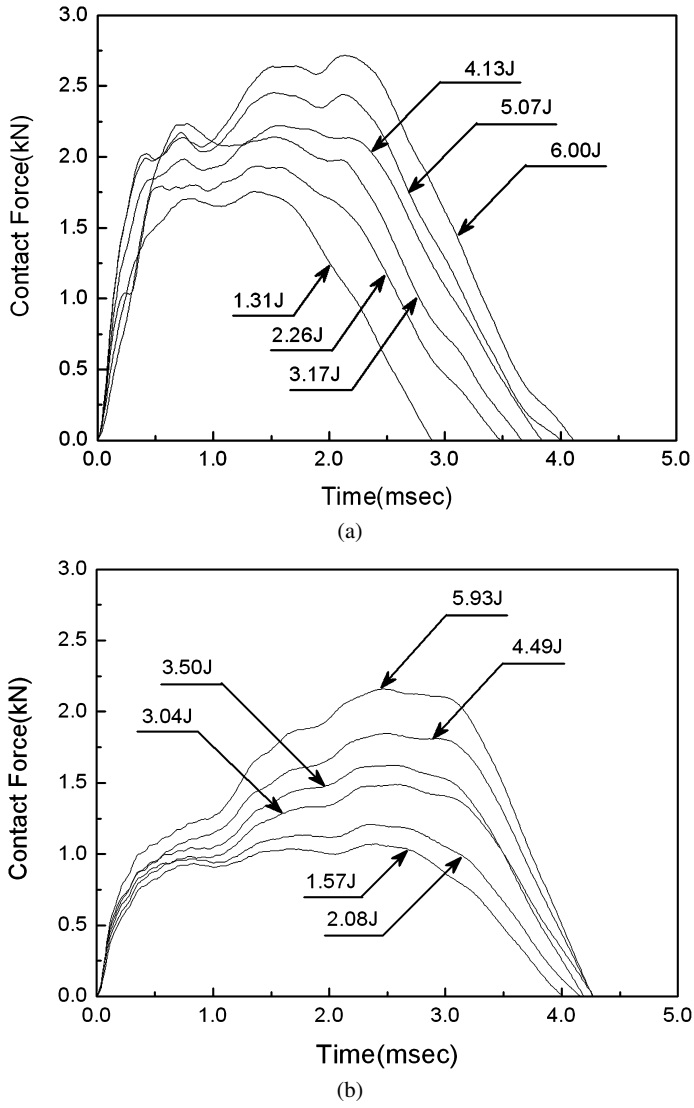

Figure 7. Force–time histories with impact energy for the sandwich specimens. (a) Body-shell sandwich panels (GE/AH) and (b) floor sandwich panels (AL/AH).

which is similar to the results of body-shell sandwich panels. When compared to the body-shell sandwich panels with woven glass fabric/epoxy laminate face-sheet, the load–time curve shows relatively smooth loading and unloading portion because there is no failure mode such as delamination and fiber breakage due to metal aluminum face-sheet. However, couple of smooth loading and unloading portion in the load–time response can be attributed to the sequential failure that occurs. The possible sequence of failure may be the residual indentation created by plastic deformation of metal aluminum face-sheet and local crushing of the core.

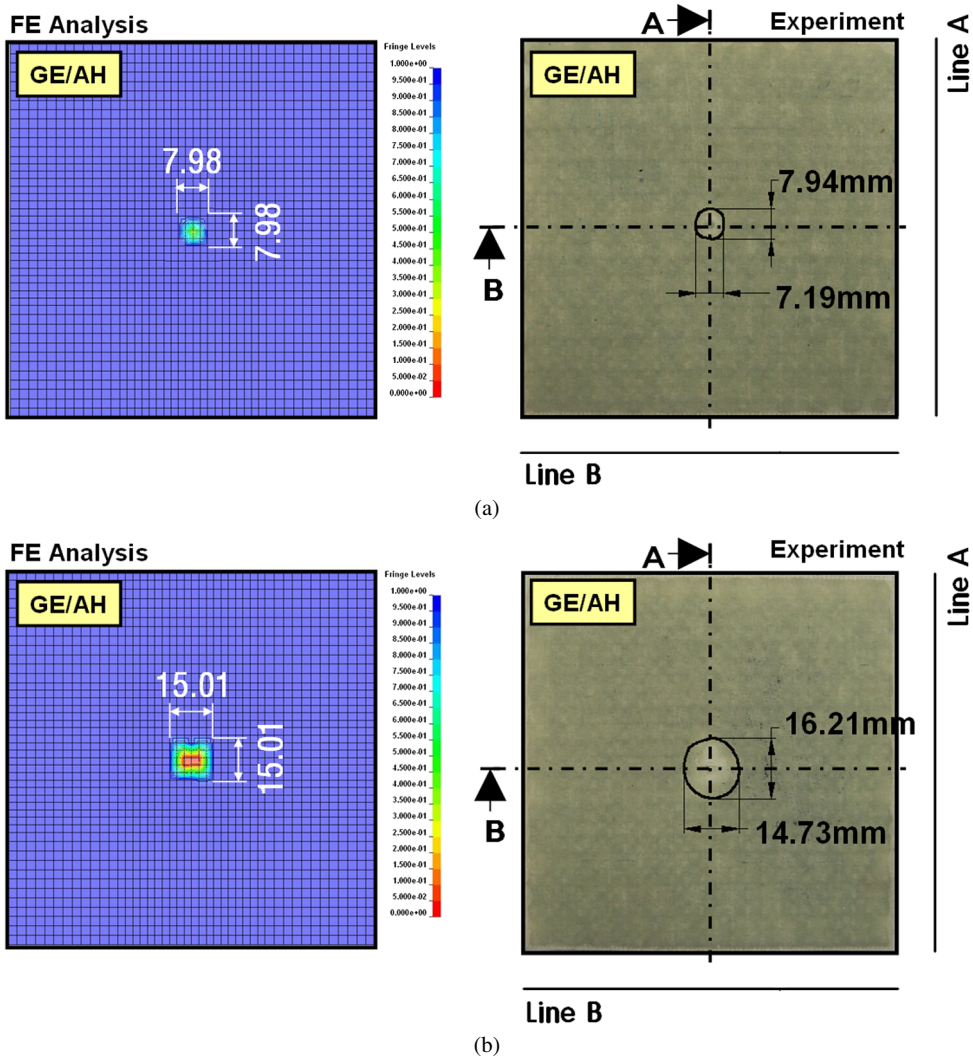

Figure 8. Comparison of impact damage areas for body-shell sandwich panels (GE/AH) after impact loading. (a) 1.31 J, (b) 3.17 J, (c) 4.07 J and (d) 5.97 J. This figure is published in color on http://www.ingentaconnect.com/content/vsp/acm

Figure 8 shows the experimental and numerical simulation results of damage areas and residual indentation created by low-velocity impact loading at 1.31 J, 3.17 J, 4.13 J and 6.00 J for body-shell sandwich specimens (GE/AH). The circle-shaped damage areas could be measured by visual inspection due to the appearance of a white color that was marked by delamination suffered by the top face-sheet made of woven glass fabric/epoxy composites. Although the circle-shaped damage areas increased with increase in impact energy for body-shell sandwich specimens (GE/AH), the residual indentation was firstly measured by 3-D scanner at impact

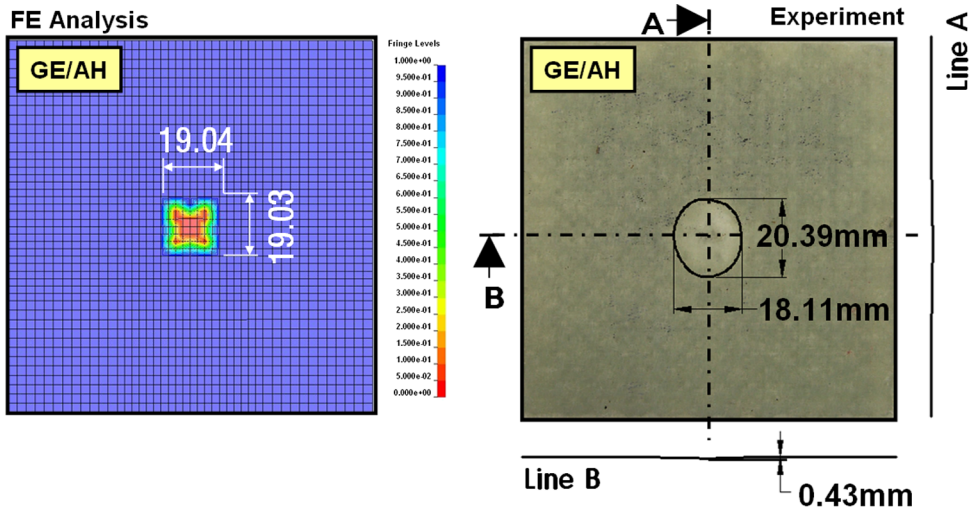

(c)

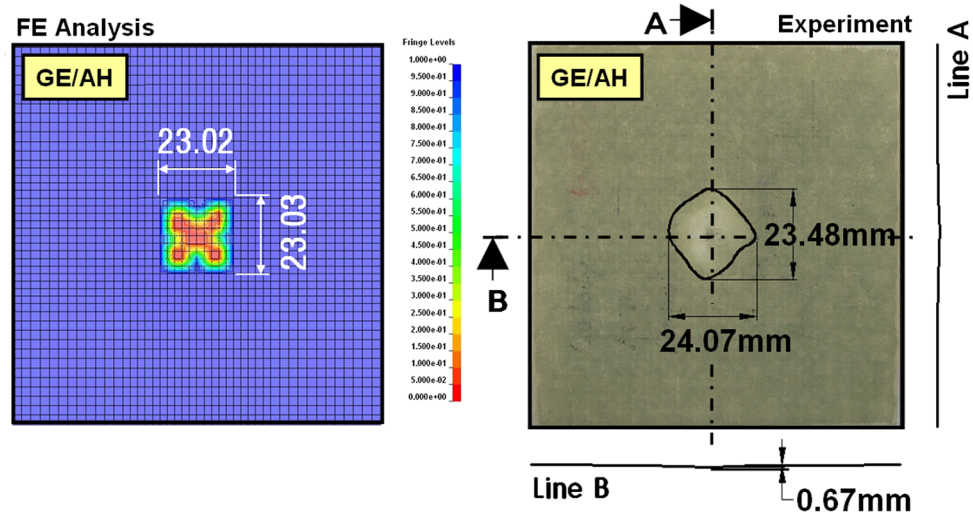

(d)

Figure 8. (Continued.)

energy of 4.13 J, which is less than 1.0 mm in depth. The plotted results of numerical simulation for damaged state are shown in the left of Fig. 8. These results were plotted using failure indicator of tensile matrix mode (e_{mt} in Table 5). A value of zero indicates no damage within the composite plies, while a value more than zero shows damage within the composite plies. Since delamination was always associated with initial matrix cracking, this failure criterion indicator was assumed to be comparable with experimental damage state.

Figure 9 shows the experimental and numerical simulation results of damage areas and residual indentation created by low-velocity impact loading at 1.57 J,

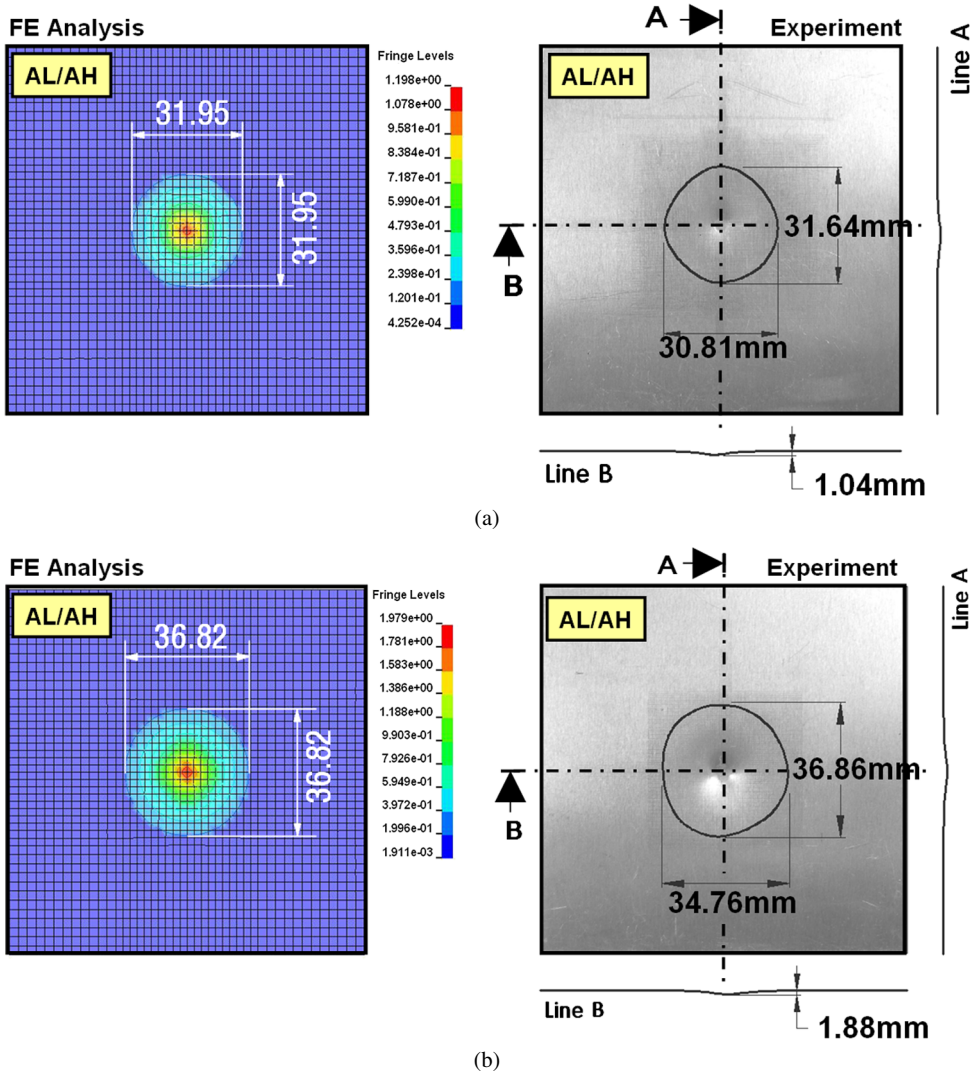

Figure 9. Comparison of impact damage areas for floor sandwich panels (AL/AH) after impact loading. (a) 1.57 J, (b) 3.04 J, (c) 4.49 J and (d) 5.93 J. This figure is published in color on http://www.ingentaconnect.com/content/vsp/acm

3.04 J, 4.49 J and 5.93 J for floor sandwich specimens (AL/AH). The depth and shape of residual indentation in experiments was measure by a 3-D scanner along line A and B as shown in the right of Fig. 9. The size of damage area and depth of permanent indentation increased with increase in impact energy for all experiments and numerical simulation. Permanent indentation in the impacted face-sheet accompanied with localized core crushing beneath and around the impact site was produced by low-velocity impact. The plotted results of numerical simulation depicted at the left of Fig. 9 are for residual plastic strain after impact. These results

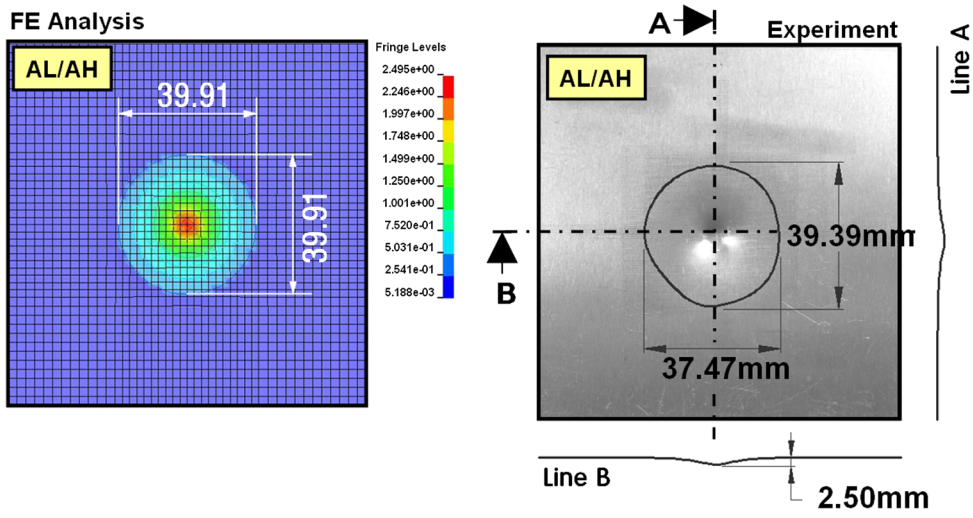

(c)

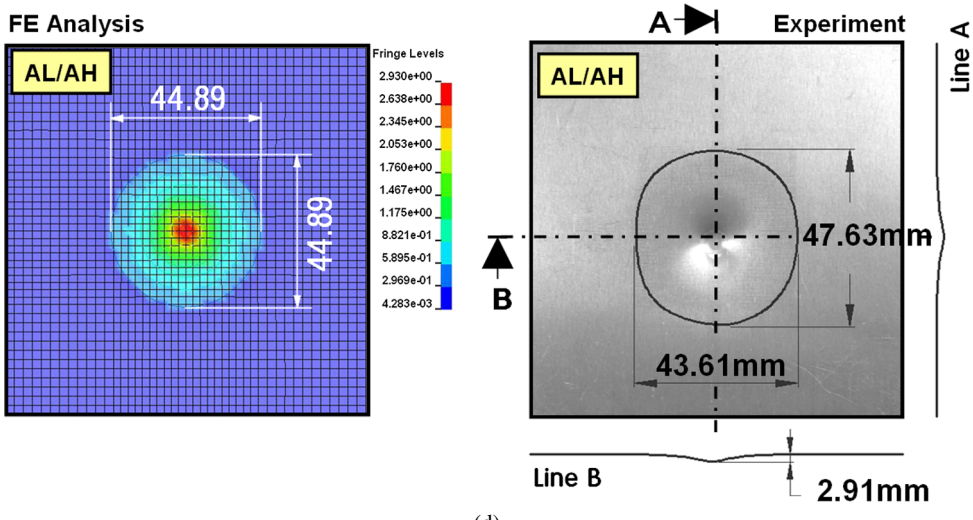

(d)

Figure 9. (Continued.)

demonstrate that both the shape and size of the face-sheet plastic strain area was predicted well by the simulation. It could be seen from the impacted specimens in Fig. 9.

Figure 10 represents the experimental and numerical simulation results of the sectioned sandwich panels with the damage produced by an impact loading. In the investigation of the post-impact damage mode, the results showed that the failure characteristics of sandwich panels were strongly dependent on the core and face-sheet materials. The body-shell sandwich panels with woven glass fabric/epoxy laminate face-sheet (GE/AH) experienced the post-damage modes such as delam-

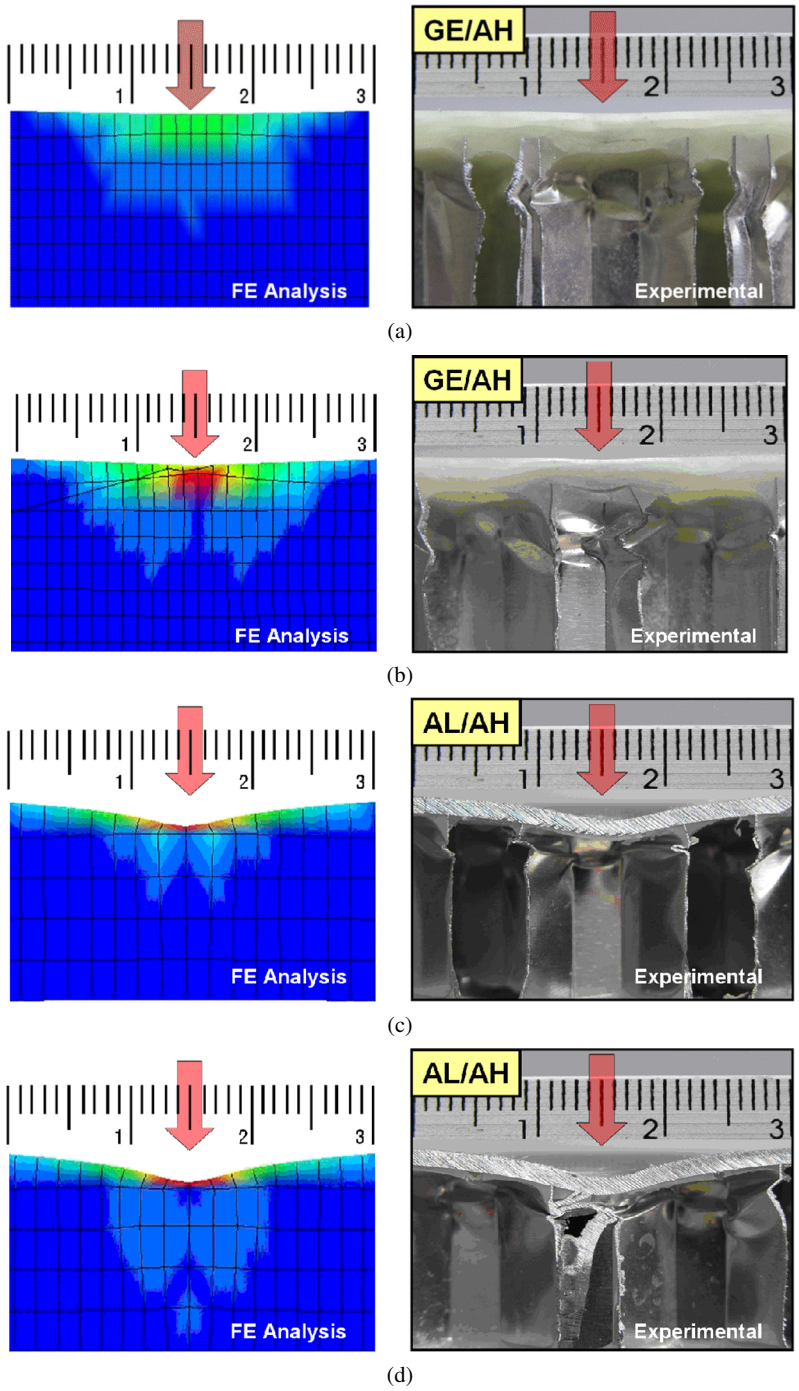

Figure 10. Comparison of post-impact damage for sectioned sandwich panels after impact loading. (a) GE/AH specimens (4.13 J), (b) GE/AH specimens (6.00 J), (c) AL/AH specimens (4.49 J) and (d) AL/AH specimens (5.93 J). This figure is published in color on http://www.ingentaconnect.com/content/vsp/acm

Table 7.
Comparison of impact response for AL/AH and GE/AH sandwich panel

AL/AH	Impact energy (J)	Dent depth (mm)			Plastic strain area (mm^2)		
		EXP	FEA	Error (%)	EXP	FEA	Error (%)
	1.31	1.04	1.19	14.42	765.38	801.33	4.70
	3.17	1.88	1.98	5.32	1006.65	1064.23	5.72
	4.13	2.50	2.49	0.40	1159.34	1250.35	7.85
	6.00	2.91	2.93	0.69	1633.73	1581.86	3.17
GE/AH	1.57	∼0	0.12	–	44.92	49.99	11.27
	3.04	∼0	0.16	–	187.87	176.86	5.86
	4.49	0.43	0.46	6.98	290.89	284.73	2.12
	5.93	0.67	0.66	1.49	443.70	415.99	6.25

ination in the top face-sheet and core crushing. The representative post-damage modes of floor sandwich panels with metal aluminum face-sheet (AL/AH) were a permanent visible indentation and core crushing. The damage area and dent depth on the body-shell and floor sandwich panel (GE/AH and AL/AH) were measured after each impact test and the results were compared with FE analysis predictions in Table 7. Numerical and experimental results showed good agreement for the damage area and the depth of indentation of sandwich composite panels created by the impact loading.

4. Conclusion

The BIMODAL tram is the development project subjected to weight limit regulations for ground transportation vehicle in Korea. The BIMODAL tram will be developed using a honeycomb sandwich structure with high stiffness-to-weight and strength-to-weight ratios to reduce the weight of its vehicle. The honeycomb sandwich panels are classified into two groups according to the applied part. One group is the body-shell sandwich panel with composite laminate face-sheet, and second group is the floor sandwich panel with metal aluminum face-sheet.

The present paper describes the results of an experimental and numerical simulation study of low-velocity impact responses on composite laminate skinned and metal aluminum skinned aluminum honeycomb sandwich panels subjected to low-velocity impact loading. The impact test was performed to understand and characterize the type and extent of the damage observed in a variety of honeycomb sandwich panels with composite laminate face-sheet and metal aluminum face-sheet. The 3-D scanner was utilized to measure quantitatively the impacted damage size and depth of the residual indentation. In 3-D scanning analysis of the top face-sheet for body-shell sandwich specimens with woven glass fabric/epoxy laminate face-sheet, the residual indentation was quite small or absent. For body-shell sandwich specimens with aluminum honeycomb core only, the residual indentation of

less than 1.0 mm in depth was measured at impact energy of 4.13 J. On the other hand, the floor sandwich panels with metal aluminum face-sheet were much damaged at even the lowest levels of impact energy and severely dented in the direction of their thickness.

A modeling approach with 3-D solid elements and 2-D shell elements was applied to honeycomb sandwich panels, which is capable of representing major sandwich failure modes. The material properties obtained by coupon tests of the respective materials were used to determine the material parameters for composite laminate and metal aluminum face-sheets and the effective equivalent damage model for the honeycomb core. The modified Chang–Chang failure criterion was used to predict matrix cracking, compressive failure and fiber breakage of the composite laminate.

Good agreement was obtained by comparing numerical simulation and experimental results; in particular, the numerical simulation was able to predict dent depth and damage areas of honeycomb sandwich panels.

Acknowledgement

The authors would like to thank the Ministry of Construction and Transportation (MOCT) for their financial support and assistance.

References

1. D. Hachenberg, C. Mudra and M. Nguyen, Folded structure an alternative core material for future sandwich concepts, in: *DGLR Conference*, pp. 17–21 (2003).
2. J. S. Kim, S. J. Lee and K. B. Shin, Manufacturing and structural safety evaluation of a composite train carbody, *Compos. Struct.* **20**, 468–476 (2007).
3. K. B. Shin, J. Y. Lee, B. J. Ryu and S. J. Lee, A study on flexural behaviors of sandwich composites with face-sheets of unequal thickness, *The Korea Soc. Railway* **10**, 201–210 (2007).
4. L. Gilmar, Composite solutions for the transportation market, *JEC Compos. Mag.* **36**, 30–32 (2007).
5. P. M. Schubel, J. J. Luo and I. M. Daniel, Low-velocity impact behavior of composite sandwich panels, *Composites, Part A: Appl. Sci. Manuf.* **36**, 1389–1396 (2005).
6. T. Anderson and E. Madenci, Experimental investigation of low-velocity impact characteristics of sandwich composites, *Compos. Struct.* **50**, 239–247 (2000).
7. D. P. W. Horrigan, P. R. Aitken and G. Moltschaniwskyj, Modeling of crushing due to impact in honeycomb sandwiches, *J. Sandwich Struct. Mater.* **2**, 131–151 (2000).
8. M. Meo, A. J. Morris, R. Vignjevic and G. Marengo, Numerical simulations of low-velocity impact on an aircraft sandwich panel, *Compos. Struct.* **62**, 353–360 (2003).
9. M. Hoo Fatt and K. Park, Dynamic models for low-velocity impact damage of composite sandwich panels, Part A: deformation, *Compos. Struct.* **52**, 235–251 (2001).
10. G. A. O. Davies, D. Hitchings, T. Besant, A. Clarke and C. Morgan, Compression after impact strength of composite sandwich panels, *Compos. Struct.* **63**, 1–9 (2004).
11. D. M. McGowan and D. R. Ambur, Damage-tolerance characteristics of composite fuselage sandwich structures with thick face-sheets, *NASA Technical Memorandum*, No. 110303.

12. A. G. Mamalis, D. E. Manolakos, M. B. Ioannidis and P. K. Kostazos, Crushing of hybrid square sandwich composite vehicle hollow body-shells with reinforced subjected to axial loading: numerical simulation, *Compos. Struct.* **61**, 175–186 (2003).
13. A. Shipsha and D. Zenkert, Compression-after-impact strength of sandwich panels with core crushing damage, *Composites, Part A: Appl. Compos. Mater.* **12**, 149–164 (2005).
14. A. Tobiei and R. Tanov, Sandwich shell finite element for dynamic explicit analysis, *Intl J. Numer. Methods Engng* **54**, 257–267 (2000).
15. M. Q. Nguyen, S. S. Jacombs, R. S. Thomson, D. Hachenberg and M. L. Scott, Simulation of impact on sandwich structures, *Compos. Struct.* **67**, 217–227 (2005).
16. A. Matzenmiller, J. Luvliner and R. L. Taylor, A constitutive model for anisotropic damage in fiber-composites, *J. Mech. Mater.* **21**, 125–152 (1995).
17. F. K. Chang and K. Y. Chang, A progressive damage model for laminated composite containing stress concentrations, *J. Compos. Mater.* **21**, 834–855 (1987).